Title

Microtubule lattice spacing governs cohesive envelope formation of tau family proteins

Journal

Nature Chemical Biology, 18(11)

ISSN

1552-4450

Authors

Siahaan, Valerie

Tan, Ruensern

Humhalova, Tereza

et al.

Publication Date

2022-11-01

DOI

10.1038/s41589-022-01096-2

Peer reviewed

HHS Public Access

Author manuscript

Nat Chem Biol. Author manuscript; available in PMC 2023 May 01.

Published in final edited form as:

Nat Chem Biol. 2022 November ; 18(11): 1224–1235. doi:10.1038/s41589-022-01096-2.

Microtubule Lattice Spacing Governs Cohesive Envelope Formation of Tau Family Proteins

Valerie Siahaan[1,6], **Ruensern Tan**[2,4,6], **Tereza Humhalova**[3], **Lenka Libusova**[3], **Samuel E. Lacey**[5], **Tracy Tan**[4], **Mariah Dacy**[4], **Kassandra M. Ori-McKenney**[4,7], **Richard J. McKenney**[4,7], **Marcus Braun**[1,7], **Zdenek Lansky**[1,7]

[1.]Institute of Biotechnology, Czech Academy of Sciences, BIOCEV, Prague West, Czech Republic

[2.]Present address: Department of Molecular and Cellular Biology, University of California at Berkeley, Berkeley, CA, USA

[3.]Department of Cell Biology, Faculty of Science, Charles University, Prague, Czech Republic

[4.]Department of Molecular and Cellular Biology. University of California – Davis. Davis CA, 95616

[5.]Structural Studies Division, MRC Laboratory of Molecular Biology, Cambridge, UK. Current: Human Technopole, Milan, Italy

[6.]Co-first authors

Abstract

Tau is an intrinsically-disordered microtubule-associated protein (MAP) implicated in neurodegenerative disease. On microtubules, tau molecules segregate into two kinetically distinct phases, consisting of either independently diffusing molecules or interacting molecules that form cohesive “envelopes” around microtubules. Envelopes differentially regulate lattice accessibility for other MAPs, but the mechanism of envelope formation remains unclear. Here, we find that tau envelopes form cooperatively, locally altering the spacing of tubulin dimers within the microtubule lattice. Envelope formation compacted the underlying lattice, whereas lattice extension induced tau-envelope disassembly. Investigating other members of the tau family, we find that MAP2 similarly forms envelopes governed by lattice-spacing, whereas MAP4 cannot.

[7.]Co-corresponding authors. KMOM: kmorimckenney@ucdavis.edu, RJM: rjmckenney@ucdavis.edu, MB: marcus.braun@ibt.cas.cz, ZL: zdenek.lansky@ibt.cas.cz.

Author Contributions Statement

The manuscript was conceptualized by R.T., K.M.O.M., R.J.M., M.B., and Z.L.; Methods were developed by V.S., T.H., L.L., S.E.L., R.J.M., M.B., and Z.L.; Recombinant proteins were generated by V.S., R.T., T.T., and M.D.; TIRF experiments were performed by V.S., R.T., and R.J.M.; Optical tweezers experiments by V.S.; CryoEM experiments by S.E.L.; Live-cell experiments by T.H.; Data was formally analyzed by V.S., R.T., T.H., S.E.L., K.M.O.M., and R.J.M.; The manuscript was written by V.S., L.L., K.M.O.M., R.J.M., M.B., Z.L., with reviewing and editing by T.T. and M.D.; The project was supervised by K.M.O.M., R.J.M., M.B., and Z.L.; Funding was acquired by V.S., T.H., L.L., K.M.O.M., R.J.M., M.B., and Z.L..

Competing Interests Statement

The authors declare no competing interests.

Statistics and reproducibility

For representative figures, whenever not specifically stated in the caption, all data was collected from at least two independent trials. All repeated independent experiments showed similar results and no data was excluded from the manuscript. Unless otherwise stated, all data were analyzed manually using ImageJ (FIJI) or Matlab (R2020b). Graphs were created using GraphPad Prism v.8.0.1 or Matlab R2020b and statistical analyses were performed using the same software. Major points on graphs represent data means and the error bars represent variation or associated estimates of uncertainty.

Envelopes differentially biased motor protein movement, suggesting that tau family members could spatially divide the microtubule surface into functionally distinct regions. We conclude that the interdependent allostery between lattice-spacing and cooperative envelope formation provides the molecular basis for spatial regulation of microtubule-based processes by tau and MAP2.

Editor summary:

Microtubule-associated proteins tau and MAP2 cooperatively form protein envelopes that compact the underlying tubulin lattice, revealing a novel role for these proteins in altering microtubule structure.

Introduction

Microtubules, polymers composed of tubulin, provide mechanical rigidity for the cell and tracks for motor-driven intracellular transport. Microtubules undergo alternating phases of polymerization and depolymerization, dependent on tubulin GTP hydrolysis activity. During polymerization, GTP-tubulin associates with the growing tip of the microtubule. After tubulin incorporation into the microtubule lattice, tubulin-bound GTP is hydrolysed to GDP. GTP hydrolysis is accompanied by a ~2.5Å longitudinal compaction of the interdimer interface within the mammalian tubulin lattice[1]. Compacted GDP-lattices can be artificially extended by microtubule stabilizing agents, such as the GTP analogue guanosine-5′-[(α,β)-methyleno]triphosphate (GMPCPP) or taxol (Paclitaxel)[1]. While GMPCPP keeps the microtubule lattice in an extended state due to its extremely low turnover[2], taxol binds transiently and increases the microtubule lattice spacing reversibly[3]. Tubulin spacing can also be altered by the interaction of microtubule-associated proteins (MAPs) with the lattice[4–6], demonstrating the dynamic interdependence between the structure of the microtubule lattice and lattice-bound proteins.

MAPs have different affinities for the compacted or extended tubulin lattice and can employ this difference as a readout for their localization on the microtubule. High affinity for the GTP-tubulin enables localization of specific MAPs to the microtubule tips[7,8]. Other MAPs, such as the kinesin-3 KIF1A or the neuronal protein tau, are reported to have a higher affinity for GDP tubulin, which enables their specific localization to the GDP regions of the microtubules[9–11].

Tau, along with MAP2 and MAP4, constitute a family of evolutionarily and structurally related, intrinsically disordered MAPs, important in neuronal development and function[12,13]. Neuronally enriched tau is associated with a number of neurodegenerative disorders termed “tauopathies”, while, to date, a role for MAP2 and MAP4 in disease has not been described[14,15]. MAP2 is mostly localized to dendrites and regulates neuronal cargo trafficking by inhibiting kinesin motors[16,17]. In contrast to tau and MAP2, MAP4 is more ubiquitously expressed in various tissues[12]. MAP4 regulates microtubule-based cargo trafficking by inhibiting dynein motility and enhancing kinesin-based transport. However, a MAP4 fragment reduced the motility of kinesin-1 and kinesin-3 *in vitro*[18–20], and overexpression of MAP4 inhibited vesicle motility *in vivo*[21]. Tau can assemble into various higher-order structures. In solution, tau undergoes liquid-liquid phase separation[22–24],

In neurons, tau aggregates into neurofibrillary tangles[25], found in Alzheimer's disease brains. When bound to microtubules, tau molecules can form oligomers[26,27] and cohesive envelopes, previously referred to as "condensates" or "islands"[9,28], which act as selectively permeable barriers for other MAPs[9,28], inhibiting kinesin motility, while allowing dynein-based motility[9,16,17,26,28,29]. The mechanism underlying the envelope formation, however, remains elusive.

Here, we found that microtubule lattice spacing governs the cooperative formation of tau envelopes. We show that this mechanism is conserved for MAP2, but not MAP4, and demonstrate functional consequences of these differential binding modes. Our results show that the regulation of MAP cooperativity through the spacing of tubulin dimers within the microtubule lattice is a divergent evolutionary feature within this family of MAPs.

Results

Tau cooperativity by local microtubule lattice compaction

To study the tau envelope formation, we immobilized taxol-stabilized microtubules on a coverslip, added purified fluorescently labelled full-length 2N4R tau, and imaged the system using total internal reflection fluorescence (TIRF) microscopy (Fig. 1a). Initially we varied tau concentration and measured the tau density on the microtubule surface, revealing that tau envelope formation is a cooperative process (Fig. 1b) with a Hill coefficient of 1.9 ± 0.7. During envelope growth we often observed straightening of microtubules (Fig. 1c, Supplementary Movie 1), suggesting that cooperative binding of tau influences the microtubule structure. Previously, we observed that tau envelopes form on GDP microtubule lattices but do not form on microtubules stabilized with GMPCPP[9]. To probe how the structure of the microtubule lattice affects tau envelope formation, we analyzed the envelope growth on (a) GMPCPP-capped GDP-lattice microtubules (natively compacted), (b) taxol-lattice microtubules (extended reversibly), and (c) GMPCPP-lattice microtubules (extended irreversibly). We observed that the rate with which tau envelopes covered the GDP-lattice microtubules (1.6 ± 1.3 μm/s; mean ± s.d) was more than an order of magnitude faster than the coverage rate on taxol-lattice microtubules (23.0 ± 12.8 nm/s; mean ± s.d), while, in agreement with previous observations[9], no envelope formation was observed on GMPCPP-lattice microtubules (Fig. 1d, Supplementary Fig. 1a–d). These results demonstrate that cooperative tau envelopes preferably form on compacted GDP-lattice microtubules.

To test if irreversible lattice extension hinders the envelope formation, even at saturating tau concentrations, we added 600 nM tau to a mixture of GMPCPP-lattice and taxol-lattice microtubules (Fig. 1e, left panels). At this concentration, tau uniformly covers the microtubule and the envelopes cannot be distinguished by local changes in tau density. However, tau envelopes can be detected by their effect on kinesin-1, which is occluded from the envelopes[28]. After the addition of 60 nM kinesin-1, we observed no movement of kinesin-1 on the taxol-lattice microtubules, showing that these were fully covered by tau envelopes (Fig. 1e, Supplementary Movie 2, Supplementary Fig. 1e,f). By contrast, on the GMPCPP-lattice microtubules, kinesin-1 moved along their entire lengths, revealing that tau did not form envelopes, even at saturating tau concentrations. Additionally, we studied dynamics of single tau molecules on GMPCPP-lattice microtubules within this elevated tau

concentration (600 nM tau-mCherry and 0.2 nM tau-meGFP) and found that 100% of single tau-meGFP molecules moved diffusively on GMPCPP-lattice microtubules (Supplementary Fig. 1g). This further reveals that tau does not form envelopes on GMPCPP-lattice microtubules, since tau molecules inside envelopes do not diffuse, but remain stationary[9,28]. Permanent extension of the microtubule lattice thus prevents envelope formation, suggesting that the microtubule lattice spacing might regulate the envelope formation.

Therefore, we reasoned that tau envelope formation might induce microtubule lattice compaction. To test this hypothesis, we employed sparsely labeled microtubules (Fig. 1f) with fluorescent speckles marking fixed positions on the microtubule. After the addition of 400 nM tau to speckled taxol-lattice microtubules, envelopes formed rapidly and we observed a decrease in the distances between the individual speckles, indicating that the microtubule lattice was compacting concomitantly with the cooperative binding of tau (Fig. 1g, Supplementary Movie 3). Repeating the experiment at lower tau concentration (20 nM), and following the compaction in- and outside the envelope regions, we found no compaction of the lattice in the regions of the microtubule not covered by tau envelopes, while the lattice regions covered by a tau envelope showed a compaction of 3.2 ± 1.0% (Fig. 1h, Supplementary Fig. 1h–k). The extent of the compaction is similar to the length difference between GTP- and GDP-bound tubulin dimers estimated previously by cryo-EM to be 2.4%[1], suggesting that tau envelopes shift tubulin from its extended GTP-like into its compacted GDP-conformation. As cooperative binding of tau to the microtubule reverses the taxol-induced lattice extension, we asked if the envelope formation will locally induce dissociation of taxanes from the microtubule. We visualized tau interaction with microtubules labelled with SiR-tubulin, a fluorogenic taxane based on docetaxel, which binds to the same site as taxol, but with a higher affinity[30]. Comparison of the SiR-tubulin intensity within or outside the tau envelope regions (Fig. 1i,j, Supplementary Movie 4) revealed a decrease of 21.7 ± 12.9% (mean ± s.d.) within the enveloped regions. These results are consistent with prior data showing competition between tau and taxol for microtubules[31]. Combined, these experiments show that a localized structural shift to the compacted GDP-tubulin microtubule lattice induces cooperative formation of tau envelopes.

Lattice extension induces disassembly of tau envelopes

Tau envelope formation induces a reversible compaction of taxol-extended tubulin. We hypothesized that physically lengthening microtubule lattices either locally or globally should induce the disassembly of tau envelopes. Locally, we extended the lattice by bending the microtubules in a hydrodynamic flow. Using GMPCPP-capped GDP-lattice microtubules attached to the coverslip at a single point, we formed tau envelopes over the entire length of the GDP-lattice. By briefly (~10 s) introducing a hydrodynamic flow, the microtubules bent at their single attachment points, extending the lattice locally on the outside of the bend point (Fig. 2a). During the hydrodynamic flow, we removed tau from solution and added either buffer alone or buffer containing 10 μM taxol to further induce lattice extension. After the period of flow, the microtubules relaxed back to their original (straight) shape. We found that, during the flow period, both in presence and absence of taxol, the tau density in the highly curved regions dropped by approximately 50% (Fig. 2b), indicating a fissure in the envelope. After the hydrodynamic flow, in the presence of 10 μM taxol in solution,

the envelopes disassembled from the ends. Additionally, the envelope started disassembling from the location where the fissure had been introduced by mechanical bending (Fig. 2a, Supplementary Movie 5) as evidenced by a drop in tau density to 3.6 ± 2.8% (Fig. 2a,b; mean ± s.d.). In the absence of taxol, the fissure closed when the microtubule relaxed, with the tau density recovering to 77.3 ± 10.8% (Fig. 2a,b, Supplementary Movie 6; mean ± s.d.). These results demonstrate that transient local extension of the lattice by mechanical means destabilizes tau envelopes.

To assess if physical extension of the entire microtubule lattice can induce tau envelope disassembly, we attached individual microtubules between two beads held in two optical traps and moved the beads apart until we began detecting a force increase. We then fixed the beads in this position, with the microtubule in a straight but non-stretched state (Fig. 2c). After adding 60 nM tau to the chamber we observed tau envelope formation (Fig. 2d) and, simultaneously, detected an increase in force due to a decrease in the distance between the two beads, indicating a compaction of the microtubule lattice (Fig. 2e,f). No compaction was detected in a control experiment when the buffer was exchanged but no tau was added (Fig. 2e, Supplementary Fig. 2a). Next, we stretched microtubules with pre-formed tau envelopes by moving the beads apart until we reached a set force of 40 pN. We then removed tau from solution and monitored the disassembly rate of the tau envelopes while keeping the force constant (Fig. 2g,h, Supplementary Movie 7). In a control experiment, we monitored the disassembly rate of tau envelopes on microtubules suspended in a relaxed, non-stretched state (Fig. 2h,i, Supplementary Movie 8). We found that the disassembly rate of tau envelopes increased 2-fold when the microtubule lattice was stretched by an external force. Combined, these experiments establish that tau envelope formation is tightly linked to microtubule mechanics, and show that physically extending microtubule lattices coated by tau envelopes induces envelope disassembly, suggesting that tau functions in living cells may be mechanosensitive.

Conservation of MAP envelope formation within the tau family

In vertebrates, the tau family also includes the neuronal MAP2 and the more ubiquitously expressed MAP4, which are conserved within their carboxy-terminal microtubule binding repeats, and differ significantly outside this region (Fig. 3a)[12,13]. To investigate whether envelope formation is conserved within the tau family, we produced MAP2c and MAP4 (Fig. 3a), and examined the behavior of these MAPs on taxol-lattice and GMPCPP-lattice microtubules (Fig. 3b). MAP2c behaved similarly to tau, forming envelopes on taxol-lattice but not on GMPCPP-lattice microtubules. Conversely, we did not observe envelope formation on either lattice with MAP4, but rather uniform binding along the microtubule length (Fig. 3b, Supplementary Fig. 3a). Quantification of MAP intensity on both types of lattices revealed that the MAP2c level outside of the envelopes was identical to that on GMPCPP-lattice microtubules, similar to tau[9]. The intensity of MAP4 was identical on either type of lattice (Fig. 3b), further suggesting that MAP4 cannot form envelopes.

We next examined these MAPs on taxol-lattices at the single molecule level. At picomolar concentrations, both MAP2c and MAP4 molecules showed predominantly diffusive interactions with microtubules (Supplementary Fig. 3a). To probe for concentration

dependent effects on single molecule behavior, we used higher concentrations of GFP-MAP2c or GFP-MAP4 and added picomolar concentrations of fluorescent TMR-labeled MAP2c or MAP4. The diffusive behavior of TMR-MAP2c outside of the GFP-MAP2c envelopes did not change with increasing concentrations of GFP-MAP2c. However, TMR-MAP2c molecules transitioned to static binding within the GFP-MAP2c envelopes (Supplementary Fig. 3a), their dwell times increasing ~3-fold (Supplementary Fig. 3a,b), as observed for tau[9,28]. In contrast, TMR-MAP4 molecules remained diffusive regardless of the concentration (Supplementary Fig. 3a), consistent with its inability to form envelopes. To further explore the dynamics of these MAPs on taxol-lattices, we performed FRAP experiments. Similar to previous observations with tau[9], MAP2c molecules turned over ~4-fold faster when they resided outside versus inside envelope boundaries (Supplementary Fig. 3c). By contrast, MAP4 showed homogenous behavior with a recovery time and mobile fraction comparable to envelope-associated MAP2c, in accordance with the observed ~2-fold longer dwell times for single MAP4 molecules versus MAP2c (Supplementary Fig. 3b).

Tau envelopes are sensitive to the aliphatic alcohol 1,6-hexanediol (1,6-HD), a compound that disrupts phase separated systems in a variety of biological contexts[9], revealing that they share some material properties with these systems. Similar to tau[9], MAP2c envelopes dissolved when exposed to 1,6-HD, but the diffusive fraction of MAP2c molecules remained unchanged (Fig. 3c, Supplementary Fig. 3b). MAP2c envelopes were not dissolved by the 1,6-HD isomer 2,5-hexanediol (Fig. 3c), revealing tau and MAP2c's sensitivity to 1,6-HD is similar to phase separated systems[32]. In contrast, 1,6-HD had no effect on the binding of MAP4 to microtubules, further demonstrating the distinct biophysical properties of MAP4 (Fig. 3c, Supplementary Fig. 3b).

We next tested the effect of MAP2c or MAP4 on microtubule lattice spacing. First, we mixed each MAP with SiR-tubulin and measured the average SiR-tubulin intensity along microtubules. Similar to tau (Fig. 1i), the presence of MAP2c decreased SiR-tubulin binding by over 3-fold, while MAP4 had no effect (Fig. 3d). We next measured microtubule compaction by tracking fluorescent speckles on taxol-lattice microtubules upon addition of MAPs (Supplementary Fig. 1j,k). Similar to tau, we observed compaction within MAP2c envelopes, but not outside (Fig. 3e). In contrast, we observed no microtubule compaction upon the addition of MAP4. To confirm these results, we performed cryo-EM analysis of taxol-microtubules in the presence of MAPs to directly measure the tubulin spacing within the lattice. Consistent with their ability to form envelopes, we found that both tau and MAP2c binding resulted in ~1Å compaction between tubulin monomers, consistent with prior cryo-EM measurements between GDP and GTP-like lattices[1] (Fig. 3f). For tau, we observed a bimodal distribution of lattice spacing, suggesting that the lattice was not covered entirely in tau envelopes under our conditions. Addition of MAP2c caused a more complete compaction, to a level consistent with the compacted tau lattice (Fig. 3f). In contrast, addition of MAP4 did not result in measurable compaction within the tubulin lattice (Fig. 3f), consistent with the rest of our observations that MAP4 does not form envelopes on microtubules.

Given their distinct modes of binding, we wondered how the three members of the tau family co-exist on microtubules. We first mixed tau with either differentially-labeled tau,

MAP2c or MAP4 and measured how enriched each molecule became within tau envelopes. As expected[9], tau was highly co-enriched within tau envelopes (Fig. 3g). Strikingly, MAP2c colocalized with the tau envelopes, where it was strongly enriched (Fig. 3g) showing that tau and MAP2c can form miscible MAP envelopes. By contrast, MAP4 was largely excluded from tau envelopes (Fig. 3g). To further confirm this result, we co-mixed all three MAPs at equimolar concentrations and observed strong co-segregation of tau and MAP2c into envelopes that excluded MAP4 into the surrounding regions (Fig. 3h). Dilution of MAP4 to single molecule levels in these conditions revealed that, while single MAP4 molecules diffused on the microtubule lattice outside of tau/MAP2c envelopes, they were unable to diffuse into the tau/MAP2c envelopes (Fig. 3h). Further, individual MAP4 molecules located within the tau/MAP2c envelopes remained static, demonstrating that tau/MAP2c envelopes exclude MAP4 at their boundaries and restrict the dynamics of MAP4 within. Combined, these data reveal that like tau, MAP2c forms envelopes, which compact an extended microtubule lattice. By contrast, MAP4 does not form cohesive envelopes in any condition tested, and is unable to affect the structure of the lattice, suggesting functional diversification within the tau family related to the ability to both recognize and alter the conformation of the microtubule lattice.

Lattice spacing governs MAP cooperativity in vivo

Our results show that compacted microtubule lattices induce cooperative binding of tau, and that extending microtubule lattices induces disassembly of tau envelopes *in vitro*. Since the majority of tubulin incorporated to microtubules *in vivo* is thought to be in the compacted GDP-state, our results suggest that the majority of tau *in vivo* is bound to microtubules cooperatively. To test this hypothesis, we aimed to induce tau envelope disassembly by extending the microtubule lattices in living cells using taxol. We imaged U-2 OS cells expressing eGFP-tau and observed that 94% of all cells (total n=18 cells, 5 experiments), covering a 20-fold range of expression levels, exhibited eGFP-tau levels high enough that microtubules were fully covered by tau. In the remaining 6% of cells, exhibiting weak eGFP-tau expression, tau only localized to the microtubule bends, as described previously[33,34]. We added 0.01 μM taxol to the medium and imaged the cells for 10 minutes while monitoring the tau density on microtubules initially fully covered by eGFP-tau. In line with our *in vitro* observations, and previous *in vivo* evidence[33,35], we observed that in all cells tau dissociated from the microtubules (Fig. 4a, Supplementary Movie 9) as quantified by the decrease in the coefficient of variation of the tau signal (Fig. 4b). Tau remained on the microtubules when only DMSO was added to the medium, and the coefficient of variation remained largely unchanged (Fig. 4a,b, Supplementary Movie 10), showing that the dissociation of tau from microtubules is specific to taxol treatment. Staining the cells for α-tubulin, or co-transfecting the cells with eGFP-tau and mScarlet-α-tubulin, verified that microtubules were not disrupted by either treatment (Supplementary Fig. 4a–c). We repeated this experiment with U-2 OS cells expressing eGFP-MAP4. In contrast to tau and in line with previous *in vivo* evidence[35], we found that MAP4 remained on the microtubules after either treatment with DMSO or taxol (Fig. 4c, Supplementary Movie 11,12), as quantified by the unchanged coefficient of variation (Fig. 4d).

Importantly, when analyzing the tau dissociation during the taxol-driven extension of the native compacted microtubule lattice, we found that the tau signal disappeared from the microtubules in patterns that resembled the disassembly of tau envelopes *in vitro*[9,28]. Without substantial changes in the initial tau density on the microtubule, fissures in the tau signal appeared, which increased in size over time. The distinct regions of tau signal formed by these fissures then disassembled from their boundaries until they disappeared, similar to tau envelope disassembly *in vitro* (Fig. 4e–g, Supplementary Fig 4d–f, Supplementary Movie 13–15). If tau would have been bound non-cooperatively, we would expect tau to unbind from the microtubules uniformly along the microtubule length, as observed for non-cooperatively bound tau *in vitro*[28]. However, in cells treated with taxol we always observed envelope-like disassembly, rather than uniform tau unbinding. We thus conclude that the vast majority of tau in U-2 OS cells was cooperatively bound to microtubules, and that artificial lattice extension by taxol reveals this cooperative binding through envelope dissolution. These results suggest that native GDP-microtubule lattices *in vivo* can be fully enclosed by tau envelopes.

MAP cooperativity differentially regulates motor proteins

We next aimed to determine the functional implications for the different microtubule binding behaviors we observed. We investigated how MAP2c and MAP4 affected the motility of the retrograde microtubule motor complex, dynein-dynactin-Hook3 (DDH), and the anterograde kinesin-3 microtubule motor, KIF1A. In our assays, DDH complexes bound and moved processively along microtubules in the absence and presence of both MAP2c and MAP4 (Fig. 5a). We found that at the highest concentrations of MAPs tested, MAP4, but not MAP2c, decreased the number of processive dynein motors on the microtubule (Fig. 5a,b). At low concentrations of MAP2c, where envelope boundaries are visible, we observed occasional pausing of DDH complexes at the envelope boundary (Fig. 5a, arrow), similar to prior observations with tau[9]. Neither MAP strongly affected the average velocity (including pauses) of these motors (Fig. 5c). We analyzed the pixel-by-pixel correlation between the averaged intensities of the MAPs and DDH (methods). We found no observable negative correlation (Fig. 5d), suggesting that neither MAP strongly affects the spatial distribution of the motors along microtubules. The modest effect of MAP4 on the DDH landing rate may be consistent with prior results[18,19], which suggested MAP4 could inhibit dynein-based movements. The landing rate of dynein-dynactin complexes is strongly determined by the $p150^{glued}$ subunit of the dynactin complex[36], and we speculate that MAP4 may directly affect the interaction of $p150^{glued}$ with the microtubule.

We next examined KIF1A, a neuronal cargo transporter critical for human health[37–40] and sensitive to the nucleotide state of the microtubule lattice[11]. KIF1A motors bound and moved along microtubules in the absence and presence of low concentrations of MAP2c and MAP4 (Fig. 5e). However, at higher concentrations these MAPs strongly decreased the number of processive motors without changing the velocity of motors that were able to bind (Fig. 5e–g). These observations indicate that both MAPs strongly affect the landing rate of the KIF1A motors. In contrast to DDH, we observed a strong spatial effect of MAP2c on KIF1A (Fig. 5e,h). The average pixel intensities of KIF1A were negatively correlated with the average intensities of MAP2c at both concentrations tested, whereas we did not observe

a negative correlation between KIF1A and MAP4 (Fig. 5h). These results indicate that cooperative envelope formation facilitates spatial regulation of the KIF1A motor along the microtubule, and demonstrate that MAP2c and MAP4 exert different effects on retrograde and anterograde motors.

Discussion

Cooperative binding of tau and MAP2c to microtubules both requires and, reciprocally, induces a local compaction of the underlying microtubule lattice. We propose to use the term “envelopes” for these microtubule-dependent structures to distinguish them from soluble tau droplets, often termed “condensates”, which form independent of the microtubule lattice [22–24]. We hypothesize that MAP-driven compaction of the lattice might allosterically alter the conformation of the regions of lattice adjoining the boundaries of the envelope. This could be mediated by the conserved microtubule-binding repeats, which span several tubulin dimers[41]. This “through the lattice” allostery might locally increase the affinity for new MAP molecules binding proximal to the envelope boundaries, as previously proposed for kinesin motors[4,6,42] and microtubule dynamics[43]. Additionally, direct MAP-MAP interactions might facilitate the preferential binding of MAP molecules at the envelope boundaries. These interactions might be mediated by the regions flanking the microtubule binding repeats of tau or MAP2, as these domains are required for envelope formation[9,28]. Additionally, our 1,6-hexanediol experiments suggest that phase separation of tau and MAP2 on the microtubule surface might contribute to cooperative envelope formation. MAP4 adopts a conformation completely distinct from that of tau[41,44] on microtubules, which may at least partially explain why, unlike tau, MAP4 is unable to form envelopes.

Our data suggests that tau and MAP2, but not MAP4, are sensitive to the mechanical state of the microtubule lattice, and thus are suited to function as mechanosensitive MAPs. This observation may have physiological relevance in muscle cells where isoforms of MAP4 are abundantly expressed, and there are several reports of tau expression in various types of muscle tissue[15,45,46]. Additionally, mechanosensitivity could be an important feature in the developing nervous system during cell polarization or cell migration.

Mammalian tubulin within the GDP lattice primarily adopts compacted state, whereas the newly incorporated GTP tubulin adopts an expanded state[1]. Intriguingly, in non-mammalian species, microtubule lattice compaction does not appear to be directly coupled to GTP hydrolysis[47,48]. Additionally, recent evidence suggests that the microtubule lattice is not conformationally homogenous, but rather releases and incorporates new GTP-tubulin subunits in response to mechanical damage and repair[49]. Thus, the microtubule lattice in living cells may not exist in a homogenously compacted, GDP state, as previously thought. We suggest it is plausible that MAPs that recognize and alter the compaction state of the lattice, such as tau and MAP2, may play active roles in biasing the conformational dynamics of tubulin within the lattice. It is presumed that the predominant volume of the microtubule lattice in cells is in the GDP compacted state, suggesting that most of tau in cells is bound to the microtubule in a cooperative manner, which is in agreement with our experimental observations *in vivo*, where tau unbound from microtubules after the addition of taxol. We occasionally observed enriched tau signal in microtubule bends, even after taxol addition,

in accordance with prior observations[9,35]. Our results suggest that this is due to tau binding to the compressed lattice on the inner side of the bends. By contrast, at high levels of tau, when the lattice is fully decorated by tau, bending of the lattice leads to local decrease in tau densities[28], which could be explained by the disruption of the tau envelope on stretched lattice on the outer side of the bend.

We demonstrate that MAP envelopes differentially regulate the motility of two predominant microtubule motor systems: dynein-based retrograde, and kinesin-based anterograde transport. Because MAP4 does not form envelopes, it is unable to provide spatially distinct regulation of motors and rather regulates them globally. However, our observation that MAP4 is excluded from tau or MAP2 envelopes raises the possibility that MAP exclusion could act as an extrinsic mechanism to spatially dictate MAP binding within cells. Such a mechanism has also been suggested for tau and MAP7, which have opposite effects on kinesin-1 motility[16]. Why are different classes of kinesin motors unable to access the microtubule lattice under MAP envelopes? Apart from steric clashes between tau and kinesin[9,41], kinesin binding expands the microtubule lattice[4,6] suggesting that exclusive binding may arise from competition for an expanded versus compacted lattice. In prior experiments, MAP4 did not block the binding of a kinesin-1 motor domain to microtubules[44], while we show that it negatively affects KIF1A motility. This distinction could be due to the dominating influence of KIF1A's k-loop on its landing rate[50]. Our data reveal that tau and MAP2 envelopes spatially gate kinesin access to the microtubule, while allowing dynein to pass. These MAPs are highly enriched within the neuronal system and this capability may be harnessed to spatially regulate microtubule-based trafficking. We hypothesize that the efficiency of cargo trafficking trough MAP envelopes is further modulated by motor associated proteins[51] and the numbers and types of different motors bound to the cargo. Colocalization of tau and MAP2 into shared envelopes that exclude MAP4 suggests that different MAPs can form spatially distinct domains on the microtubule lattice, differentially regulating access to microtubule surface. Our work raises the hypothesis that the heterogeneity of the MAP envelope may thus provide a means for sectioning the microtubule surface into functionally distinct segments.

Methods

Microtubule Assembly

Porcine brains were obtained from a local abattoir and used within ~4 h of death. Porcine brain tubulin was isolated using the high-molarity PIPES procedure then labeled with biotin NHS ester, Dylight-405 NHS ester, Alexa-647 NHS ester, or Atto-647 ester as described previously[52,53]. Biotin-labeled tubulin as well as HiLyte647-labeled tubulin were purchased from Cytoskeleton Inc. (T333P and TL670M, respectively).

Taxol-lattice microtubules (GTP polymerized, then taxol stabilized; stored and imaged in presence of taxol) were polymerized from 4 mg/ml tubulin for 30 min at 37 °C in BRB80 (80mM PIPES, 1mM EGTA, 1mM $MgCl_2$, pH 6.9) supplemented with 4 mM $MgCl_2$, 5% DMSO, and 1mM GTP (Jena Bioscience, NU-1012). The polymerized microtubules were diluted in BRB80T (BRB80 supplemented with 10μM taxol (paclitaxel)) and centrifuged for

30 min at 18000 x g in a Microfuge 18 Centrifuge (Beckman Coulter). After centrifugation the pellet was resuspended and kept in BRB80T.

GMPCPP-lattice microtubules (GMPCPP polymerized) were polymerized from 4 mg/ml tubulin for 2 h at 37 °C in BRB80 supplemented with 1mM $MgCl_2$ and 1mM GMPCPP (Jena Bioscience, NU-405). The polymerized microtubules were centrifuged for 30 min at 18000 x g in a Microfuge 18 Centrifuge (Beckman Coulter). After centrifugation the pellet was resuspended and kept in BRB80T.

GMPCPP-capped GDP-lattice microtubules (GTP polymerized, GMPCPP-capped) were polymerized from 4 mg/ml tubulin for 30 min at 37 °C in BRB80supplemented with 4 mM $MgCl_2$, 5% DMSO, and 1mM GTP (Jena Bioscience, NU-1012). The polymerized microtubules were centrifuged at 37 °C for 30 min at 18000 x g in a Microfuge 18 Centrifuge (Beckman Coulter). After centrifugation, the pellet was resuspended and incubated for 20 min at 37 °C in BRB80 supplemented with 100 mM $MgCl_2$, 10mM GMPCPP and 0.25 mg/ml tubulin for cap formation.

Speckled microtubules were polymerized as taxol-lattice microtubules prepared from 4 mg/ml tubulin comprised of 2% biotin-labeled tubulin and 0.133% Atto647-labeled tubulin.

Protein Constructs and Purification

For *in vitro* experiments comparing tau-family proteins, tau and MAP2c constructs were cloned into pET28A vectors using Gibson assembly. Full-length human MAP4 (isoform 1) was codon optimized for insect cell expression by Epoch Biosciences before cloning into the pFastbac vector. All constructs contain an N-terminal cassette consisting of a 6xHis-tag, tandem Strep-tags, and fluorophore or SNAPf tag connected by a GS-linker as previously described[9]. *Mus musculus* MAP2c was acquired from the Ori-McKenney lab[16].

For *in vitro* experiments, tau[9,22],MAP2c[16], Dynein-dynactin-Hook3 complexes[54], a truncated, constitutively dimerized Kif1A construct[16], and kinesin-1-GFP[51] were expressed and purified as previously described..

MAP4 was expressed in insect cells using the Bac-to-Bac system (Thermo Fisher). Cells were infected at ~2 million cells/ml for 60 hours before harvesting. Cells were resuspended in lysis buffer (50mM Tris pH8, 150mM K-acetate, 2mM $MgSO_4$, 1mM EGTA, 10% glycerol) with protease inhibitor, 1mM DTT, 1mM PMSF, 1% Triton X-100, and DNaseI, and dounced on ice. Cell lysate, after douncing, was cleared by centrifugation at 14,000 xg for 20 min, and loaded onto Streptactin Superflow resin (Qiagen) and extensively washed with lysis buffer. Bound proteins were eluted with 3mM desthiobion (sigma) in lysis buffer. Eluted proteins were loaded on cation exchange column 5ml HiTrapS (GE Healthcare) in lysis buffer pH7.5 and eluted with 0-0.6M NaCl gradient over 40 column volumns. Fractions were collected, concentrated, and flash frozen in LN_2.

SNAPf-tagged MAP proteins were labeled by incubation with 2-5 μM SNAP dye at 4°C for ~ 2-4 hours. Unbound dye was removed by passage through a HiTrap desalting column equilibrated in GF150 buffer (25mM HEPES pH 7.4, 150mM KCl, 1mM $MgCL_2$). Protein

was concentrated using Amicon Ultra concentrators (Millipore) and flash frozen in liquid nitrogen and stored at −80°C.

TIRF microscopy

Total internal reflection fluorescence (TIRF) microscopy experiments were performed on an inverted microscope (Nikon-Ti E, Nikon-Ti2 E) equipped with 60x or 100x NA 1.49 oil immersion objectives (Apo TIRF or SR Apo TIRF, respectively, Nikon) and either Hamamatsu Orca Flash 4.0 sCMOS or PRIME BSI (Teledyne Photometrics) cameras. Or on either of two custom-built through-the-objective TIRF microscope based on a Nikon Ti-E or Ti-2 microscope body, motorized ASI or Nikon stage, quad-band filter cube (Chroma), laser launch (100 mW, 405 nm; 150 mW, 488 nm; 100 mW, 560 nm; 100 mW, 642 nm), EMCCD camera (iXon Ultra 897) and a high-speed filter wheel (Finger Lakes Instruments)[9]. Microtubules and MAPs were visualized sequentially by switching between microscope filter cubes for Cy5, TRITC and FITC channels or by using a quad band set filter (405/488/561/640). All imaging was performed using a ×100 1.45 NA objective (Nikon) and if necessary, the ×1.5 tube lens setting was used. The microscopes were controlled using Micro-Manager 1.4 or Nikon NIS Elements software. All experiments were conducted at room temperature, if required the sample chamber was kept at 25°C using an objective warmer (Oko Labs).

TIRF chambers were assembled from acid-washed coverslips as described previously (http://labs.bio.unc.edu/Salmon/protocolscoverslippreps.html) and double-sided sticky tape. Chambers were first incubated with 0.5 mg ml^{-1} PLL-PEG-biotin (Surface Solutions) for 10 min, followed by 0.5 mg ml^{-1} streptavidin for 5 min. Or TIRF chambers were assembled from coverslips silanized with 0.05% dichlorodimethylsilane (DDS, #440272, Sigma) and thin strips of parafilm melted in between two coverslips, as described previously[51]. The chambers were first incubated with 20 μg/ml anti-biotin antibodies (#B3640, Sigma) for 5 minutes, followed by 1% F127 (#P2443, Sigma, 1% in PBS) for at least 30 minutes.

MTs were diluted into BC Buffer (80 mM PIPES pH 6.8, 1 mM $MgCl_2$, 1 mM EGTA, 1 mg ml^{-1} BSA, 1 mg ml^{-1} casein and 10 μM taxol) or BRB80T (80mM PIPES, 1mM EGTA, 1mM MgCl2, pH 6.9, 10μM taxol) then incubated in the chamber and allowed to adhere to the streptavidin-coated surface for 10 min or the antibody-coated surface for 1 min. Unbound MTs were washed away with TIRF assay buffer AB1 (60 mM HEPES pH 7.4, 50 mM potassium acetate, 2 mM $MgCl_2$, 1 mM EGTA, 10% glycerol, 0.5% Pluronic F-127, 0.1 mg ml^{-1} biotin-BSA, 0.2 mg ml^{-1} κ-casein and 10 μM taxol) or BRB80T. Unless otherwise stated, experiments were conducted in imaging buffer IB1 (AB1 supplemented with 2 mM Trolox, 2 mM protocatechuic acid, ~50 nM protocatechuate-3,4-dioxygenase and 2 mM ATP) or assay buffer AB2 (50 mM HEPES pH 7.4, 1 mM EGTA, 2 mM $MgCl_2$, 75 mM KCl, 10 mM dithiothreitol, 0.02 mg/ml casein, 10 μM taxol, 1 mM Mg–ATP, 20 mM D-glucose, 0.22 mg/ml glucose oxidase and 20 μg/ml catalase). All experiments were quantified by pooling data from at least two chambers performed on multiple days.

FRAP experiments.—FRAP experiments were carried out largely as described previously [9]. For the FRAP experiments, chambers were sealed at both sides with vacuum grease. A

pre-bleach image was acquired by averaging 12 consecutive images. Then, 8 regions were bleached (1 empty background, 1 unbleached portion of the MT, 3 envelopes and 3 lattice or 6 regions on the MT in the case of MAP4) at 2% power without scanning; 5 images were taken before stimulation and 91 images were taken after stimulation, all at 1 s intervals. The FRAPed regions were then background subtracted using the empty background region, then normalized to the unbleached portion of the MT, and then to the average of the first 12 consecutive images of each region. N is defined as the number of bleached regions.

Kinesin-1 on GMPCPP/taxol-lattice MTs.—GMPCPP- and taxol-lattice microtubules were immobilized on the antibody-coated coverslips surface. 600 nM tau-mCherry diluted in AB2 was added to the microtubules prior to addition of kinesin-1-GFP and incubated for at least 2 minutes to ensure envelope formation. After incubation, 60 nM kinesin-1-GFP was added to the microtubules in presence of 600 nM tau, diluted in imaging buffer. Imaging of kinesin-1-GFP was performed with 20 ms or 50 ms framerate.

Lattice expansion TIRF assay.—DDS-coated coverslips were incubated with low anti-β-tubulin antibody concentration (#T7816, Sigma, 1 μg/ml in PBS) to ensure low binding of microtubules to the coverslip surface. GMPCPP-capped GDP-lattice microtubules were flushed into the measurement chamber and unbound microtubules were removed with BRB80. 20 nM tau-mCherry diluted in AB2 was added to the microtubules and incubated for 1-2 minutes. After incubation, tau was removed from the measurement chamber by introducing 20 μl of tau in AB2 either in presence or absence of taxol (0 or 10 μM taxol).

SiR-tubulin assay.—For the data in Fig. 1i, taxol-lattice microtubules were prepared as described above and kept in BRB80T-S (BRB80T supplemented with 2 μM SiR-tubulin (#SC002, tebu-bio)). SiR-tubulin-lattice microtubules were immobilized on the coverslip surface and unbound microtubules were removed with BRB80T-S. Prior to the experiment, the solution was exchanged by AB3 (AB2 supplemented with 2 μM SiR-tubulin and lacking taxol). Finally, tau in AB3 was added to the measurement chamber at the final assay concentration stated in the main text.

For the data in Fig. 3d, taxol-lattice 405- and biotin-labeled microtubules were prepared as described above and kept in BRB80 supplement with 10 μM taxol. For each chamber, microtubules were diluted at least 100-fold into AB1 lacking taxol but including 1 μM SiR-tubulin (Cytoskeleton inc.) and the mixture was allowed to bind to coverslips for 10 min. After this, the indicated amount of MAP protein in AB1 and 1 μM SiR-tubulin was flown into the chamber and MAPs were allowed to bind for 10 min before images were acquired.

1,6-hexanediol and envelope enrichment assays.—For 1,6-hexanediol experiments, 0.5 nM GFP-MAP2c or GFP-MAP4 was flowed into the chamber and imaged after a 5-minute incubation. Then a solution of 0.5 nM GFP-MAP2c or GFP-MAP4 in 10%-hexanediol in AB1 was introduced into the chamber and imaged after a 5-minute incubation. For envelope enrichment assays, 0.5 nM GFP-tau and 0.5 nM mScarlet-tau was incubated in the chamber for 5 minutes, then a mixture of 0.5 nM mScarlet-tau and 0.5nM sfGFP-tau, or sfGFP-MAP2c, or sfGFP-MAP4 was flowed into the chamber and allowed to incubate

for 5 minutes. The mScarlet–tau envelopes were used as fiducials for envelope boundaries. Background-subtracted mean intensities were obtained for a line scan along the MT. Each straight and uninterrupted (no MT overlaps) stretch of MT was counted as a single data point. Data points from two different protein preparations of mScarlet–tau envelopes were pooled. Fold enrichment was calculated by dividing each data point for envelope intensity by the average value of associated lattice intensity.

Optical tweezers

Optical trapping assay.—Correlative force measurements and microscopy were performed on an optical tweezers setup equipped with confocal fluorescence imaging and microfluidic system (c-Trap, LUMICKS B.V.). The microfluidic system was passivated by BSA (#A0281, Sigma, 0.1% in PBS) and F127 (#P2443, Sigma, 1% in PBS) no later than 100 hours before the experiment. The trap stiffness was calibrated using force calibration (0.5.1) in Bluelake (v1.6.11, LUMICKS B.V.) under zero flow condition. The experiments were performed at room temperature. Data was obtained using the Bluelake software (v1.6.11) and analyzed using FIJI, Matlab (R2020b), and Jupyterlab (0.35.4). Forces were measured along the microtubule. Distance were measured between the beads from edge to edge (center to center measurement, subtracted by 1x the diameter of the bead).

Microtubule lattice compaction (OT).—Two streptavidin silica beads (1.12 μm, #SVSIP-10-5, Spherotech) were captured in two separate traps. The beads were moved to the microtubule channel with fluorescently labeled taxol-lattice microtubules in AB4 (AB2 supplemented with 30 μM taxol), where a microtubule was specifically attached to both beads. This construct was then moved to a channel containing AB4 where the beads were slowly moved apart until an increase in the force was detected. The microtubule was then kept in a straight but unstretched position and the flow was minimized (0.01-0.02 bar). The construct was moved into the channel containing 60 nM tau-mCherry in AB4 where the compaction of the microtubule was detected by the increase in force concomitant with a decrease in the distance between the two beads. In a control experiment, the construct was moved into a channel containing AB4 in the absence of tau. The distance between two beads was measured by averaging the distance before adding tau and averaging the distance when maximum compaction was achieved.

Envelope disassembly rate.—A microtubule was suspended between two beads and moved to a channel containing 60 nM tau-mCherry in AB4. The microtubule was kept in the channel for at least 1 minute to allow tau envelope formation, and moved the beads slowly apart until 40 pN force was measured (0 pN in the control experiment). The construct was then moved into the channel containing AB4 in absence of tau where the tau envelopes disassembled under a constant flow (0.1 bar). In the experiment where external force was applied, the force was kept constant by a feedback loop moving the beads further apart while the microtubule relaxed during tau envelopes disassembly. The envelopes were imaged using confocal microscopy and the envelope length was measured using ImageJ and divided by the time it took for the full envelope to disassemble.

Image analysis

Microscopy data were analyzed using ImageJ 2.3.0/1.53q (FIJI)[57]. The background was subtracted using the 'subtract background' function with a rolling ball radius of 50 and brightness and contrast settings were modified linearly. In images with substantial drift, the 'Descriptor-based series registration (2D/3D+T)' plugin was used in FIJI with interactive brightness and size detections in the MT channel to register the images.

Tau density estimation.—Tau density on the microtubules was measured in FIJI by drawing a rectangle around the microtubule and measuring the RawIntDen. For background-subtraction the rectangle was then moved to an area directly adjacent to the microtubule where no microtubule is present and the RawIntDen was measured again and subtracted from the RawIntDen on the microtubule.

Hill coefficient analysis.—The tau density (estimated as described above) on taxol-lattice microtubules was plotted against the tau concentration. The Hill coefficient was obtained by fitting this plot using Matlab curve fitting tool using the Hill equation and weights defined as 1/stdev.

Coverage rate analysis.—Microtubules with different lattices were polymerized as described above. 20 nM tau diluted in imaging buffer AB2 (without taxol for GMPCPP- and GDP-lattice experiments) was added to the measurement chamber and the length of the tau envelopes was measured after 5 minutes of incubation time on the taxol- and GMPCPP lattice microtubules. For GDP-lattice microtubules, the coverage rate was measured by taking the full length of the GDP-lattice and dividing it by the time when the entire lattice was covered by a tau envelope.

Kinesin run length and landing rate.—Kinesin run lengths were measured manually by determiningthe beginning and the end of the run using kymographs compiled in FIJI (*KymographBuilder* plugin). Landing rates were determined by counting the number of traces within 30 seconds on various lengths of microtubules. Traces were considered when they visually resembled kinesin-1 landings (based on intensity and size).

Microtubule lattice compaction (For Fig. 1h,3e).—Compaction of the microtubule lattice was measured using speckled microtubules (see above). MAPs were added at concentrations where microtubules would be partially covered with MAP envelopes. In the case of MAP4, 20nM was added. Fluorescence images were taken with 5s framerate and individual fluorescent speckles were tracked using FIESTA tracking software (v1.6.0) to obtain the distance between two neighboring speckles. Compaction was measured by averaging the distance between two neighboring speckles before MAPs were added (average of 3-5 frames) and compared to the distance between the same speckles after 5 minutes of MAP incubation (average of 3-5 frames). Subsequently, fluorescence images of the MAPs were used to correlate the position of the speckles to the position of the envelopes on the microtubule lattice. The compaction was then averaged per microtubule for all events within tau envelopes, as well as outside tau envelopes. For MAP4, no assigning was required and

all distances between speckles were pooled into the same category (‘total’) and the average was taken from all regions per microtubule.

Analysis of DDH and KIF1A motility.—Kymographs of motor motility were analyzed manually to extract velocity and landing rate data. For velocity, entire visible runs were analyzed, including any pauses. For landing rates, the numbers of processive motors in each kymograph were counted manually. Processive runs were counted if the run was at least 3 pixels (~ 300 nm) long. For pixel-by-pixel intensity correlation between MAPs and motors, average intensity images were generated in each channel using FIJI and analyzed as described previously[16].

CryoEM characterization of microtubule lattice compaction

For CryoEM experiments, 20 μM unlabeled porcine brain tubulin (Cytoskeleton #T240) was polymerized at 37°C for 2 hours in BRB80 (80mM PIPES pH 6.8, 1mM $MgCl_2$, 1mM EGTA) supplemented with 3mM GTP. An equal volume of BRB80 supplemented with 10 μM taxol was added, and the polymerized microtubules were left at room temperature overnight. Directly prior to grid preparation, the microtubules were pelleted at 20000 rcf for 10 minutes and resuspended to 3 μM in fresh BRB80.

Microtubules and MAPs were pre-incubated before being added to EM grids. A mixture of 3 μL 3 μM microtubules and 8 μL MAP was incubated at room temperature for 20 minutes. For the microtubule-only dataset, the MAP was replaced with BRB80. Final MAP concentrations were 27 μM tau, 28 μM MAP2c, and 34 μM MAP4. During incubation, R1.2/1.3 Au300 Quantifoil EM grids were glow-discharged for 40 seconds. Then, 4 μL of the microtubule-MAP mixture was applied to the grid in a Vitrobot Mark II (TFS) set to 100% humidity and 22°C. After 30s, the grid was blotted for 4.5s and plunged into liquid ethane. The grids were loaded into a Polara cryo-electron microscope (TFS) operating at 300kV. Images were collected semi-automatically in SerialEM with a pixel size of 1.35Å/px, defocus ranging from −2 to −3 μm, and a dose rate of $25e^{-1}$/px/second for a 1.5 second exposure. ~40 images were taken for each dataset. Movie stacks were aligned in MotionCorr2 [55]. Straight and uninterrupted microtubule segments longer than 2.5 μm were then manually picked in RELION 3.0 [56], with the coordinates used to crop out each microtubule. In FIJI[57], each MT segment was then rotated to line up with the Y-axis of the image and the FFT was calculated. The spatial frequency of the peak in intensity of the 4 nm (J_s) reflection [58], corresponding to the longitudinal lattice spacing, was measured manually in FIJI.

Live-cell experiments

Molecular cloning.—The sequence of eGFP-tau was subcloned from the vector pSP6 EGFP-tau to the pcDNA4.0/TO mammalian expression vector using BamHI and AscI restriction enzymes. The sequence of the resulting pcDNA4.0/TO_EGFP-tau plasmid was checked using Sanger sequencing. The sequence coding MAP4 gene was amplified from cDNA generated from the U-2 OS cell line. The amplified fragment was then cloned into the pEGFP-C1 mammalian expression vector using the restriction enzymes HindIII and XbaI. We confirmed that the sequence of the amplified gene corresponds to the

RefSeq NM_002375.5 with Sanger sequencing. The resulting plasmid was named pEGFP-C1_MAP4.

Cell culture and preparation for live-cell experiments.—U-2 OS cells (ATCC, HTB-96) were maintained in DMEM + GlutaMAX (Sigma-Aldrich, 61965-026) supplemented with 10% FBS at 37°C in 5% CO2. Two days before imaging, the cells were plated onto 4-chamber Glass Bottom Dish (Cellvis, D35C4-20-1.5-N) to achieve 30% confluency. On the following day, the cells were transfected with the mammalian expression vector pcDNA4.0/TO_EGFP-tau or pEGFP-C1_MAP4, or co-transfected with the pcDNA4.0/TO_EGFP-tau and pmScarlet-i alphaTubulin-C1 expression vectors using the HP-Xtreme transfection reagent (Sigma-Aldrich, 636624400). The pmScarlet-i_alphaTubulin_C1 was a gift from Dorus Gadella (Addgene plasmid #85047; http://n2t.net/addgene:85047; RRID:Addgene_85047). The cells were imaged 24h after transfection, with DMEM medium exchanged for FluoroBright DMEM medium (Sigma-Aldrich, A1896701).

Live-cell imaging.—Using TIRF microscopy, cells were imaged for 1 minute before addition of taxol or DMSO, with frame interval 700 ms, or 1400 ms for dual imaging experiments. Then imaging was paused, and taxol or DMSO was added to the medium. The final concentration of taxol was 0.01 μM. Cells were recorded for an additional 10 minutes immediately after the addition of taxol or DMSO.

Immunofluorescence.—After taxol treatment, the recorded cells were fixed directly in a Glass Bottom Dish using 3% Paraformaldehyde in MSB buffer. The cells were then permeabilized with 0.1% Triton Tx-100 and subsequently stained with DM1A antibody against α-tubulin (1:500 dilution, # T9026, Sigma). Cells were then kept in the MSB buffer and imaged with the TIRF microscope.

Image analysis.—All images and movies were processed in FIJI. The two movies resulting from one recording (one movie before and one movie after the addition of taxol or DMSO) were merged. The shift resulting from manipulating the sample was corrected with the plugin Template_Matching and function Align_slices in stacks. The kymograph was generated with the KymographBuilder plugin.

***Coefficient of variation* (CoV).—**Using FIJI, a box was drawn inside the cell, covering (most of) the area of the cell. The CoV was determined from the standard deviation of the tau or MAP4 fluorescent signal within the box divided by the mean, before and 10 minutes after taxol or DMSO treatment. The CoV 10 minutes after treatment was then normalized to the CoV before treatment.

Envelope fission frequency and disassembly rate.—The fission frequency and disassembly rate of envelopes on microtubules in eGFP-tau cells were measured using FIJI. Fissions were manually counted and divided by the length of the microtubule at the time the first fission appeared until all tau envelopes had disassembled from the microtubule lattice. The length of the microtubule or envelope were obtained by the eGFP-tau signal.

Supplementary Material

Refer to Web version on PubMed Central for supplementary material.

Acknowledgements

The authors thank members of the MOM lab for feedback and discussion during the project and the Protein Facility of MPI-CBG and Veronika Váňová for technical support. We also thank Andrew Carter for critical reading of the manuscript, Ondřej Kučera for establishing the optical tweezers assay and Jan Sabó for support in obtaining imaging data. This work was supported by Czech Science Foundation grant 19-27477X to Z.L. and L.L. and grant 20-04068S to M.B.. We acknowledge the financial support from the Charles University Grant Agency (GAUK no. 373821 to V.S.) and the project “Grant Schemes at CU” (reg. no. CZ.02.2.69/0.0/0.0/19_073/0016935) to T.H. and V.S., grants 1R35GM124889 to R.J.M. and 1R35GM133688 to K.M.O.M.. K.M.O.M. is also supported by the Pew Charitable Trusts grant A19-0406. We acknowledge the institutional support from the CAS (RVO: 86652036), CMS supported by MEYS CR (LM2015043), and the Imaging Methods Core Facility at BIOCEV, an institution supported by the MEYS CR (Large RI Project LM2018129 Czech-BioImaging) and ERDF (project no. CZ.02.1.01/0.0/ 0.0/16_013/0001775) for their support in obtaining imaging data presented in this paper.

Data availability

Source data files for all figures and supplementary figures, are available with this manuscript.

References

1. Alushin GM et al. High-Resolution Microtubule Structures Reveal the Structural Transitions in αβ-Tubulin upon GTP Hydrolysis. Cell 157, 1117–1129 (2014). [PubMed: 24855948]
2. Hyman AA, Salser S, Drechsel DN, Unwin N & Mitchison TJ Role of GTP hydrolysis in microtubule dynamics: information from a slowly hydrolyzable analogue, GMPCPP. Mol. Biol. Cell 3, 1155–1167 (1992). [PubMed: 1421572]
3. Díaz JF, Barasoain I & Andreu JM Fast Kinetics of Taxol Binding to Microtubules: Effects of Solution Variables and Microtubule-associated proteins. J. Biol. Chem 278, 8407–8419 (2003). [PubMed: 12496245]
4. Peet DR, Burroughs NJ & Cross RA Kinesin expands and stabilizes the GDP-microtubule lattice. Nat. Nanotechnol 13, 386–391 (2018). [PubMed: 29531331]
5. Zhang R, LaFrance B & Nogales E Separating the effects of nucleotide and EB binding on microtubule structure. Proc. Natl. Acad. Sci 115, E6191–E6200 (2018). [PubMed: 29915050]
6. Shima T et al. Kinesin-binding–triggered conformation switching of microtubules contributes to polarized transport. J. Cell Biol 217, 4164–4183 (2018). [PubMed: 30297389]
7. Maurer SP, Bieling P, Cope J, Hoenger A & Surrey T GTPγS microtubules mimic the growing microtubule end structure recognized by end-binding proteins (EBs). Proc. Natl. Acad. Sci 108, 3988–3993 (2011). [PubMed: 21368119]
8. Zanic M, Stear JH, Hyman AA & Howard J EB1 Recognizes the Nucleotide State of Tubulin in the Microtubule Lattice. PLoS One 4, e7585 (2009). [PubMed: 19851462]
9. Tan R et al. Microtubules gate tau condensation to spatially regulate microtubule functions. Nat. Cell Biol 21, 1078–1085 (2019). [PubMed: 31481790]
10. Castle BT, McKibben KM, Rhoades E & Odde DJ Tau Avoids the GTP Cap at Growing Microtubule Plus-Ends. iScience 23, 101782 (2020). [PubMed: 33294790]
11. Guedes-Dias P et al. Kinesin-3 Responds to Local Microtubule Dynamics to Target Synaptic Cargo Delivery to the Presynapse. Curr. Biol 29, 268–282 (2019). [PubMed: 30612907]
12. Dehmelt L & Halpain S The MAP2/Tau family of microtubule-associated proteins. Genome Biol. 6, 1–10 (2005).
13. Sündermann F, Fernandez M & Morgan R An evolutionary roadmap to the microtubule-associated protein MAP Tau. BMC Genomics 17, (2016).

14. Götz J, Halliday G & Nisbet RM Molecular Pathogenesis of the Tauopathies. Annu. Rev. Pathol. Mech. Dis 14, 239–261 (2019).
15. Li L, Zhang Q, Lei X, Huang Y & Hu J MAP4 as a New Candidate in Cardiovascular Disease. Front. Physiol 11, 1044 (2020). [PubMed: 32982783]
16. Monroy BY et al. A Combinatorial MAP Code Dictates Polarized Microtubule Transport. Dev. Cell 53, 60–72 (2020). [PubMed: 32109385]
17. Seitz A et al. Single-molecule investigation of the interference between kinesin, tau and MAP2c. EMBO J. 21, 4896–4905 (2002). [PubMed: 12234929]
18. Semenova I et al. Regulation of microtubule-based transport by MAP4. Mol. Biol. Cell 25, 3119–3132 (2014). [PubMed: 25143402]
19. Samora CP et al. MAP4 and CLASP1 operate as a safety mechanism to maintain a stable spindle position in mitosis. Nat. Cell Biol 13, 1040–1050 (2011). [PubMed: 21822276]
20. Karasmanis EP et al. Polarity of Neuronal Membrane Traffic Requires Sorting of Kinesin Motor Cargo during Entry into Dendrites by a Microtubule-Associated Septin. Dev. Cell 46, 204–218.e7 (2018). [PubMed: 30016622]
21. Bulinski JC, McGraw TE, Gruber D, Lan Nguyen H & Sheetz MP Overexpression of MAP4 inhibits organelle motility and trafficking in vivo. J. Cell Sci 110, 3055–3064 (1997). [PubMed: 9365275]
22. Hernández-Vega A et al. Local Nucleation of Microtubule Bundles through Tubulin Concentration into a Condensed Tau Phase. Cell Rep. 20, 2304–2312 (2017). [PubMed: 28877466]
23. Zhang X et al. The proline-rich domain promotes Tau liquid-liquid phase separation in cells. J. Cell Biol 219, e202006054 (2020). [PubMed: 32997736]
24. Zhang X et al. RNA stores tau reversibly in complex coacervates. PLOS Biol. 15, e2002183 (2017). [PubMed: 28683104]
25. Iqbal K, Liu F & Gong C-X Tau and neurodegenerative disease: the story so far. Nat. Rev. Neurol 12, 15–27 (2016). [PubMed: 26635213]
26. Dixit R, Ross JL, Goldman YE & Holzbaur ELF Differential regulation of dynein and kinesin motor proteins by tau. Science (80-.). 319, 1086–1089 (2008).
27. McVicker DP, Hoeprich GJ, Thompson AR & Berger CL Tau interconverts between diffusive and stable populations on the microtubule surface in an isoform and lattice specific manner. Cytoskeleton 71, 184–194 (2014). [PubMed: 24520046]
28. Siahaan V et al. Kinetically distinct phases of tau on microtubules regulate kinesin motors and severing enzymes. Nat. Cell Biol 21, 1086–1092 (2019). [PubMed: 31481789]
29. Chaudhary AR, Berger F, Berger CL & Hendricks AG Tau directs intracellular trafficking by regulating the forces exerted by kinesin and dynein teams. Traffic 19, 111–121 (2018). [PubMed: 29077261]
30. Diaz JF & Andreu JM Assembly of purified GDP-tubulin into microtubules induced by taxol and taxotere: Reversibility, ligand stoichiometry, and competition. Biochemistry 32, 2747–2755 (1993). [PubMed: 8096151]
31. Kar S, Fan J, Smith MJ, Goedert M & Amos LA Repeat motifs of tau bind to the insides of microtubules in the absence of taxol. EMBO J. 22, 70–77 (2003). [PubMed: 12505985]
32. Lin Y et al. Toxic PR Poly-Dipeptides Encoded by the C9orf72 Repeat Expansion Target LC Domain Polymers. Cell 167, 789–802.e12 (2016). [PubMed: 27768897]
33. Samsonov A, Yu J-Z, Rasenick M & Popov SV Tau interaction with microtubules in vivo. J. Cell Sci 117, 6129–6141 (2004). [PubMed: 15564376]
34. Balabanian L, Berger CL & Hendricks AG Acetylated Microtubules Are Preferentially Bundled Leading to Enhanced Kinesin-1 Motility. Biophys. J 113, 1551–1560 (2017). [PubMed: 28978447]
35. Ettinger A, van Haren J, Ribeiro SA & Wittmann T Doublecortin Is Excluded from Growing Microtubule Ends and Recognizes the GDP-Microtubule Lattice. Curr. Biol 26, 1549–1555 (2016). [PubMed: 27238282]
36. McKenney RJ, Huynh W, Vale RD & Sirajuddin M Tyrosination of α-tubulin controls the initiation of processive dynein–dynactin motility. EMBO J. 35, 1175–1185 (2016). [PubMed: 26968983]

37. Lam AJ et al. A highly conserved 310 helix within the kinesin motor domain is critical for kinesin function and human health. Sci. Adv 7, (2021).
38. Budaitis BG et al. Pathogenic mutations in the kinesin-3 motor KIF1A diminish force generation and movement through allosteric mechanisms. J. Cell Biol 220, (2021).
39. Chiba K et al. Disease-associated mutations hyperactivate KIF1A motility and anterograde axonal transport of synaptic vesicle precursors. Proc. Natl. Acad. Sci 116, 18429–18434 (2019). [PubMed: 31455732]
40. Boyle L et al. Genotype and defects in microtubule-based motility correlate with clinical severity in KIF1A-associated neurological disorder. Hum. Genet. Genomics Adv 2, 100026 (2021).
41. Kellogg EH et al. Near-atomic model of microtubule-tau interactions. Science (80-.). 360, 1242–1246 (2018).
42. Wijeratne SS, Fiorenza SA, Subramanian R & Betterton MD Motor guidance by long-range communication through the microtubule highway. bioRxiv (2020) doi:10.1101/2020.12.23.424221.
43. Kim T & Rice LM Long-range, through-lattice coupling improves predictions of microtubule catastrophe. Mol. Biol. Cell 30, 1451–1462 (2019). [PubMed: 30943103]
44. Shigematsu H et al. Structural insight into microtubule stabilization and kinesin inhibition by Tau family MAPs. J. Cell Biol 217, 4155–4163 (2018). [PubMed: 30275105]
45. Gu Y, Oyama F & Ihara Y Tau is widely expressed in rat tissues. J. Neurochem 67, 1235–1244 (1996). [PubMed: 8752131]
46. Shults NV et al. Tau Protein in Lung Smooth Muscle Cells. J. Respir 1, 30–39 (2020).
47. Howes SC et al. Structural differences between yeast and mammalian microtubules revealed by cryo-EM. J. Cell Biol 216, 2669–2677 (2017). [PubMed: 28652389]
48. Chaaban S et al. The Structure and Dynamics of C. elegans Tubulin Reveals the Mechanistic Basis of Microtubule Growth. Dev. Cell 47, 191–204 (2018). [PubMed: 30245157]
49. Triclin S et al. Self-repair protects microtubules from destruction by molecular motors. Nat. Mater 20, 883–891 (2021). [PubMed: 33479528]
50. Soppina V & Verhey KJ The family-specific K-loop influences the microtubule on-rate but not the superprocessivity of kinesin-3 motors. Mol. Biol. Cell 25, 2161–2170 (2014). [PubMed: 24850887]
51. Henrichs V et al. Mitochondria-adaptor TRAK1 promotes kinesin-1 driven transport in crowded environments. Nat. Commun. 2020 111 11, 1–13 (2020).

Methods References

52. Gell C et al. Purification of Tubulin from Porcine Brain. Methods Mol. Biol 777, 15–28 (2011). [PubMed: 21773918]
53. Tan R, Foster PJ, Needleman DJ & McKenney RJ Cooperative Accumulation of Dynein-Dynactin at Microtubule Minus-Ends Drives Microtubule Network Reorganization. Dev. Cell 44, 233–247 (2018). [PubMed: 29401420]
54. McKenney RJ, Huynh W, Tanenbaum ME, Bhabha G & Vale RD Activation of cytoplasmic dynein motility by dynactin-cargo adapter complexes. Science 345, 337–41 (2014). [PubMed: 25035494]
55. Zheng SQ et al. MotionCor2: anisotropic correction of beam-induced motion for improved cryo-electron microscopy. Nat. Methods 14, 331–332 (2017). [PubMed: 28250466]
56. Zivanov J et al. New tools for automated high-resolution cryo-EM structure determination in RELION-3. Elife 7, e42166 (2018). [PubMed: 30412051]
57. Schindelin J et al. Fiji: an open-source platform for biological-image analysis. Nat. Methods 9, 676–682 (2012). [PubMed: 22743772]
58. Chrétien D, Kenney JM, Fuller SD & Wade RH Determination of microtubule polarity by cryo-electron microscopy. Structure 4, 1031–1040 (1996). [PubMed: 8805589]

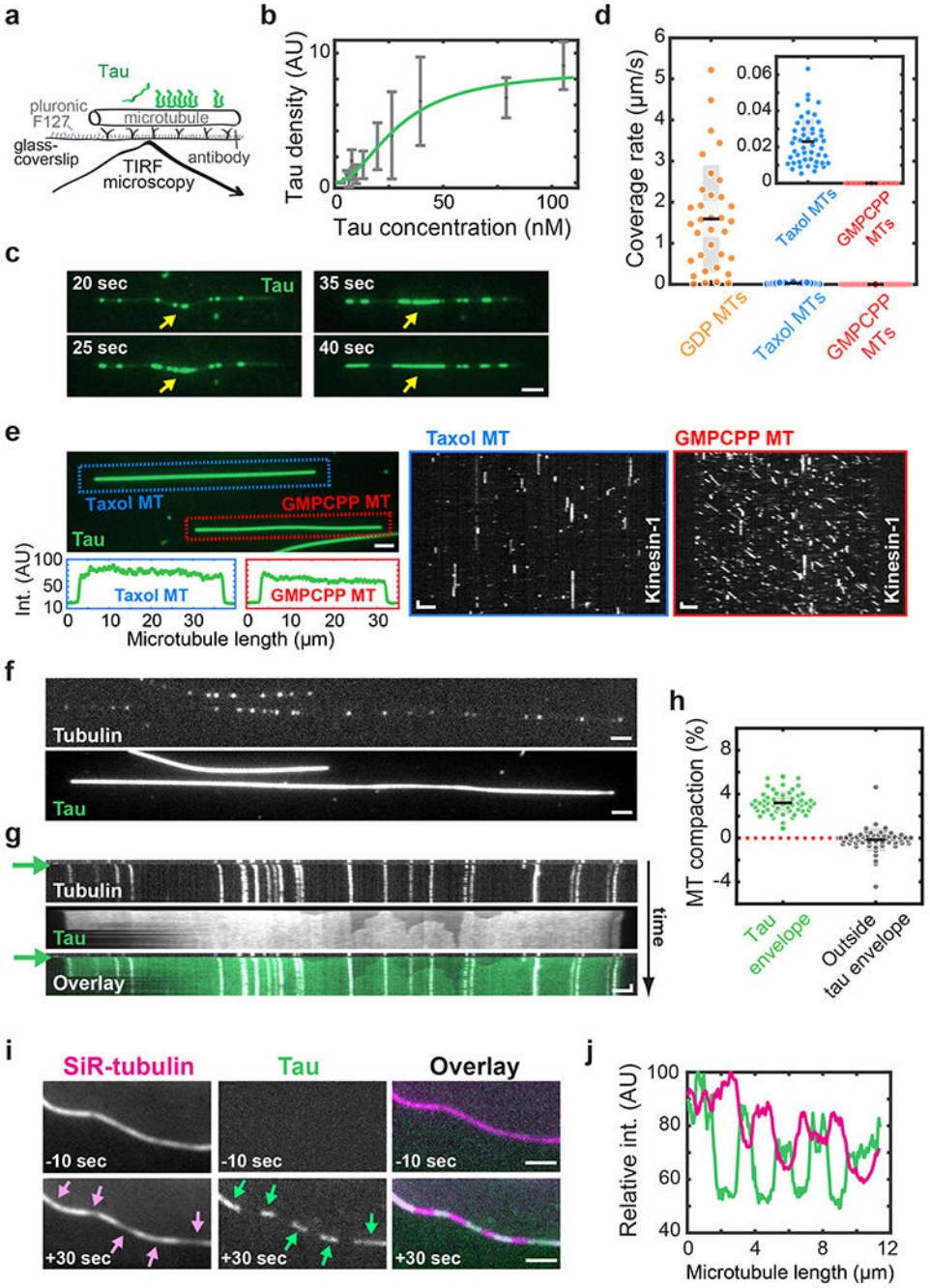

Figure 1: Tau cooperativity through local microtubule lattice compaction.

a. Schematics of the assay geometry. **b.** Quantification of cooperative binding of tau to taxol-lattice microtubules (mean ± s.d., n=652 microtubules, 60 experiments, 95% confidence bounds, r-square = 0.9633, grey), Hill-Langmuir equation fit (green). **c.** Fluorescence time lapse micrographs showing microtubule lattice straightening (yellow arrow) upon formation of tau envelopes (green). 20 nM tau-mCherry was added at t=0 sec. Scale bar: 2 μm. **d.** Rate of increase of tau envelope microtubule coverage (Methods) on different lattices after the addition of 20 nM tau-mCherry. Coverage rate was 1.6 ± 1.3 μm/s (mean ± s.d.,

n=34 microtubules, 5 experiments) on GDP-lattice microtubules (orange), 23.0 ± 12.8 nm/s (mean ± s.d., n=49 microtubules, 3 experiments) on taxol-lattice microtubules (blue) and no envelope formation (n=200 microtubules, 14 experiments) on GMPCPP-lattice microtubules (red). **e.** Fluorescence micrograph (top left) showing a taxol-lattice microtubule (marked by a blue dotted rectangle) and a GMPCPP-lattice microtubule (marked by a red dotted rectangle) after the addition of 600 nM tau-mCherry (green) and 60 nM kinesin-1-GFP. Fluorescence intensity profile along the microtubule length (bottom left) shows that the tau-mCherry density is comparable on both microtubules. Fluorescence kymographs (right panels) show that kinesin-1-GFP does not processively move on taxol-lattice microtubules (left) and moves on GMPCPP-lattice microtubules (right). Scale bars: vertical 1s, horizontal 2 μm. **f.** Fluorescence micrograph of a speckled Atto647-labeled microtubule (top) after the addition of 400 nM tau-meGFP (bottom). Scale bar: 2 μm. **g.** Multichannel kymograph corresponding to the microtubule in **f** showing compaction of the microtubule lattice - individual speckles (white) move closer to each other after the addition of 400 nM tau-meGFP (green). Addition of tau-meGFP is marked by green arrows. Scale bars: 2 μm, 1 min. **h.** Compaction of the microtubule lattice by tau within the envelope regions (3.2 ± 1.1%, mean ± s.d., n=59 envelope regions, 7 experiments) and outside the envelope regions (−0.1 ± 1.1%, mean ± s.d., n=57 microtubules, 7 experiments). **i.** Fluorescence micrographs of 2 μM SiR-tubulin (magenta) on a microtubule lattice before and after the addition of 20 nM tau-mCherry (green) at t=0 sec. Green arrows indicate tau envelopes. Pink arrows indicate the corresponding local decrease in the SiR-tubulin density. Local decrease in tau density within tau envelope regions was 21.7 ± 12.9% (mean ± s.d., n=72 envelopes, 5 experiments). Scale bar: 2 μm. **j.** Fluorescence intensity profile of SiR-tubulin (magenta) and tau-mCherry (green) on the microtubule lattice shown in **i**.

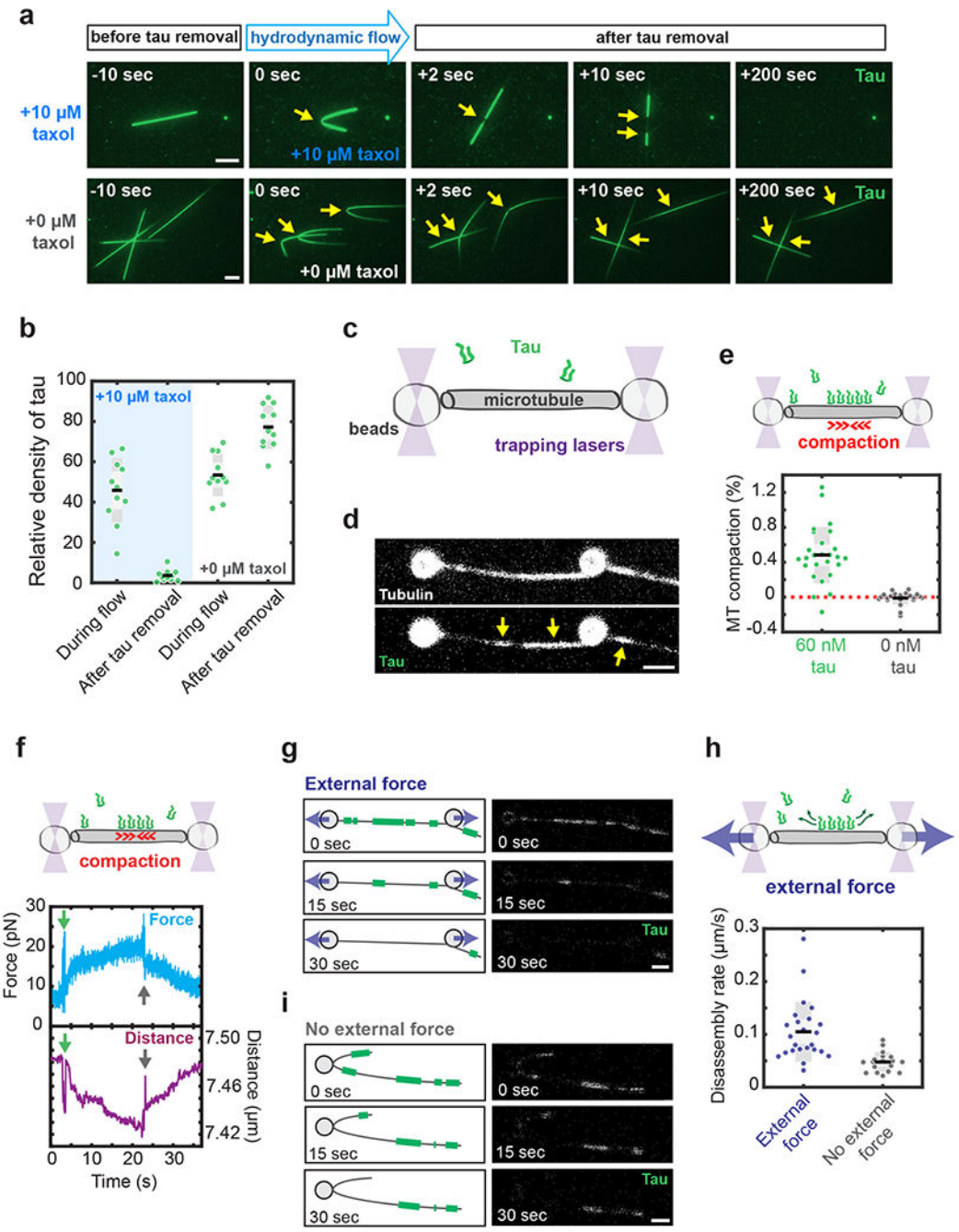

Figure 2: Lattice expansion induces disassembly of tau envelopes.

a. Fluorescence micrographs of tau-mCherry envelopes on GMPCPP-capped GDP-lattice microtubules before, during, and after hydrodynamic flow removing tau at t=0 sec. During the hydrodynamic flow we either added 10 μM taxol (top panels) or kept the measurement buffer taxol-free (bottom panels). Yellow arrows indicate the location of the bend induced by the flow and the subsequent local decrease in tau density. Scale bars: 5 μm. **b.** Relative density of tau-mCherry in the bend of GMPCPP-capped GDP-lattice microtubules, during and after the flow. With taxol in solution the density dropped to 45.9 ± 15.9% during

flow (mean ± s.d., n = 11 microtubules, 5 experiments) and decreased further to 3.6 ± 2.8% after flow (mean ± s.d., n = 11 microtubules, 5 experiments). Without taxol in solution the density dropped to 53.5 ± 10.4% during hydrodynamic flow (mean ± s.d.; n=11 microtubules, 4 experiments) and recovered to 77.3 ± 10.8% after flow (mean ± s.d.; n=11 microtubules, 4 experiments). **c.** Schematics of the optical tweezers assay. **d.** Fluorescence micrographs of a biotin-HiLyte647-labeled taxol-lattice microtubule suspended between two beads after addition of 60 nM tau-mCherry. Yellow arrows indicate locations of the tau envelopes. Scale bar: 2 μm. **e.** Compaction of taxol-lattice microtubules measured after the addition of either 60 nM tau-mCherry (green) or 0 nM tau-mCherry (grey). Compaction with tau in was 0.48 ± 0.32% (mean ± s.d., n = 26 microtubules, 26 experiments). Without tau in solution the microtubule did not compact; −0.01 ± 0.07% (mean ± s.d., n = 23 microtubules, 23 experiments, two-sided t-test, $p<0.001$). **f.** Representative force-time (blue) and distance-time (purple) graphs of a single taxol-lattice microtubule after addition of 60 nM tau-mCherry. After tau addition (green arrow) a decrease in the distance and an increase in the force is detected. After tau was removed from the channel (grey arrow) an increase in the distance, and a decrease in the force is detected, indicating relaxation of the microtubule lattice as tau envelopes disassembled. **g.** Fluorescence micrographs of tau envelope disassembly where the microtubule is stretched using external force. Sketches of the micrographs (left panels) indicate the size and positions of the tau envelopes (green lines). Scale bars: 2 μm. **h.** Disassembly rate of tau envelopes on taxol-lattice microtubules either stretched by an external force (blue, 0.11 ± 0.06 μm/s, mean ± s.d., n = 24 microtubules, 24 experiments) or relaxed when no external force is applied (grey, 0.05 ± 0.02 μm/s, mean ± s.d., n = 18 microtubules, 18 experiments, two-sided t-test, $p<0.001$). **i.** Fluorescence micrographs of a tau envelope disassembly experiment where the microtubule is relaxed in absence of external force. Sketches of the micrographs (left panels) indicate the sizes and positions of the tau envelopes (green lines). Scale bars: 2 μm.

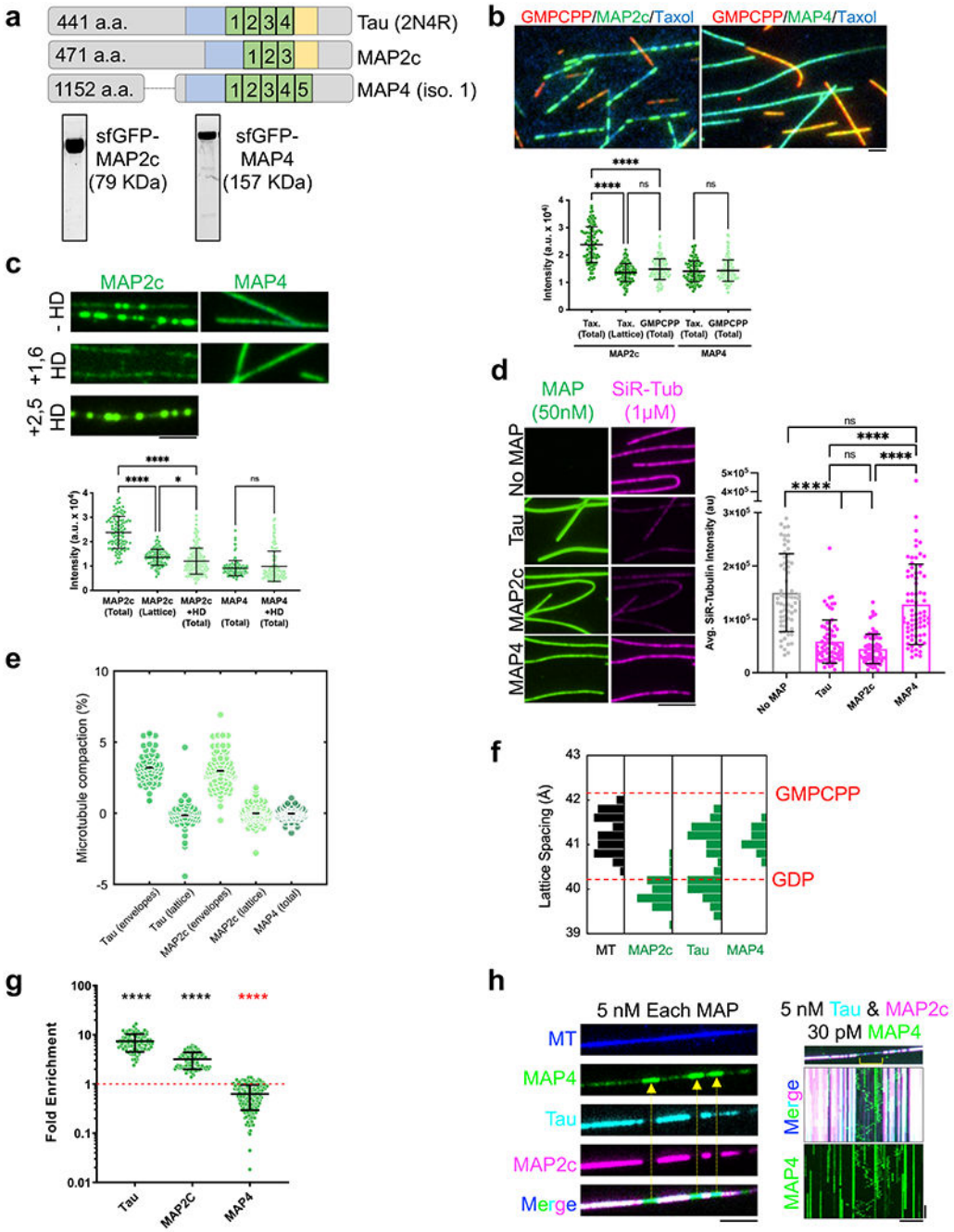

Figure 3: Cooperative envelope formation is a divergent property within the tau-family.

a. Schematics of the MAP proteins analyzed, highlighting the conserved microtubule-binding regions (green), proline-rich region (blue), and pseudo-repeat (yellow). Below: Coomassie stained gels showing purity of the MAP2c and MAP4 proteins used. See Source Data for the uncropped gels. **b**. Multi-channel fluorescence micrographs showing the binding of 0.5 nM GFP-MAP2c or GFP-MAP4 (green) to either taxol-lattice (blue) or GMPCPP-lattice microtubules (red). Note the clear formation of envelopes by MAP2c on taxol-lattice, but not on GMPCPP-lattice microtubules. Below: quantification of the

fluorescence intensity of MAPs on the indicated lattices (mean ± s.d., n = 108, 134, 116, 106, 150 microtubule segments in 3 chambers each.). 'Total' refers to the intensity on the entire lattice including regions outside and inside envelopes for MAP2c. Scale bar: 2 μm. One-way ANOVA, **** indicates p<0.001 **c.** Fluorescence images of 0.25 nM GFP-MAP proteins on taxol-lattice microtubules in the absence or presence of 10% 1,6-hexanediol or 2,5-hexanediol (HD). Below: quantification of the fluorescence intensity of MAPs in the indicated conditions (mean ± s.d., n=108, 134, 199, 146, 125 microtubule segments, respectively, 2 experiments each). One-way ANOVA, **** indicates p<0.001. **d.** Example fluorescence images showing GFP-MAP (green) and SiR-tubulin (magenta) signals along microtubules. Right: quantification of average SiR-tubulin fluorescence intensity (mean ± s.d., n=65, 74, 72, 70 microtubule segments, respectively, 2 experiments each). One-way ANOVA, **** indicates p<0.001. **e**. Compaction of the microtubule lattice measured on speckled microtubules (same method as data presented in Fig. 1h) after the addition of MAPs. For MAP2c, compaction was 3.0 ± 1.1 % in the envelope regions and 0.0 ± 0.6 % on the lattice outside the envelopes (mean ± s.d., n= 78 envelopes, n=95 lattices, in 5 experiments). For MAP4, compaction was 0.0 ± 0.4 % (n = 105 microtubules in 11 experiments). **f.** Quantification of the tubulin monomer spacing from cryo-EM images of taxol-lattice microtubules in the absence or presence of the indicated MAPs (n=46, 36, 44, 61, 30 microtubules, respectively). Red lines denote previously reported tubulin spacing for the indicated lattices[5]. **g.** Quantification of the enrichment of GFP-MAPs, based on fluorescence intensity, within mScarlet-2N4R tau envelopes (mean ± s.d., n=97, 115, 94, 112, 206, and 183 tau envelopes, respectively, 2 experiments each). 0.5 nM MAP protein was used for each condition. Note that MAP4 values below 1 indicates the protein is excluded from tau envelopes (red asterisks). One-way ANOVA, **** indicates p<0.001. **h**. Multi-channel fluorescence micrograph showing all three orthogonally-labeled MAPs mixed together on microtubules. Arrows denote the exclusion of MAP4 from the regions enriched with both tau and MAP2c. Scale bar: 5 μm. Right: TIRF image showing a single microtubule coated in tau/MAP2c envelopes. Kymograph below shows the behavior of single MAP4 molecules (green) visualized at a lower concentration, revealing that they diffuse outside (yellow bracket) but not inside tau/MAP2c envelopes (cyan & magenta). N = 2 experiments. Kymograph scale bars: 5 μm, 10 sec.

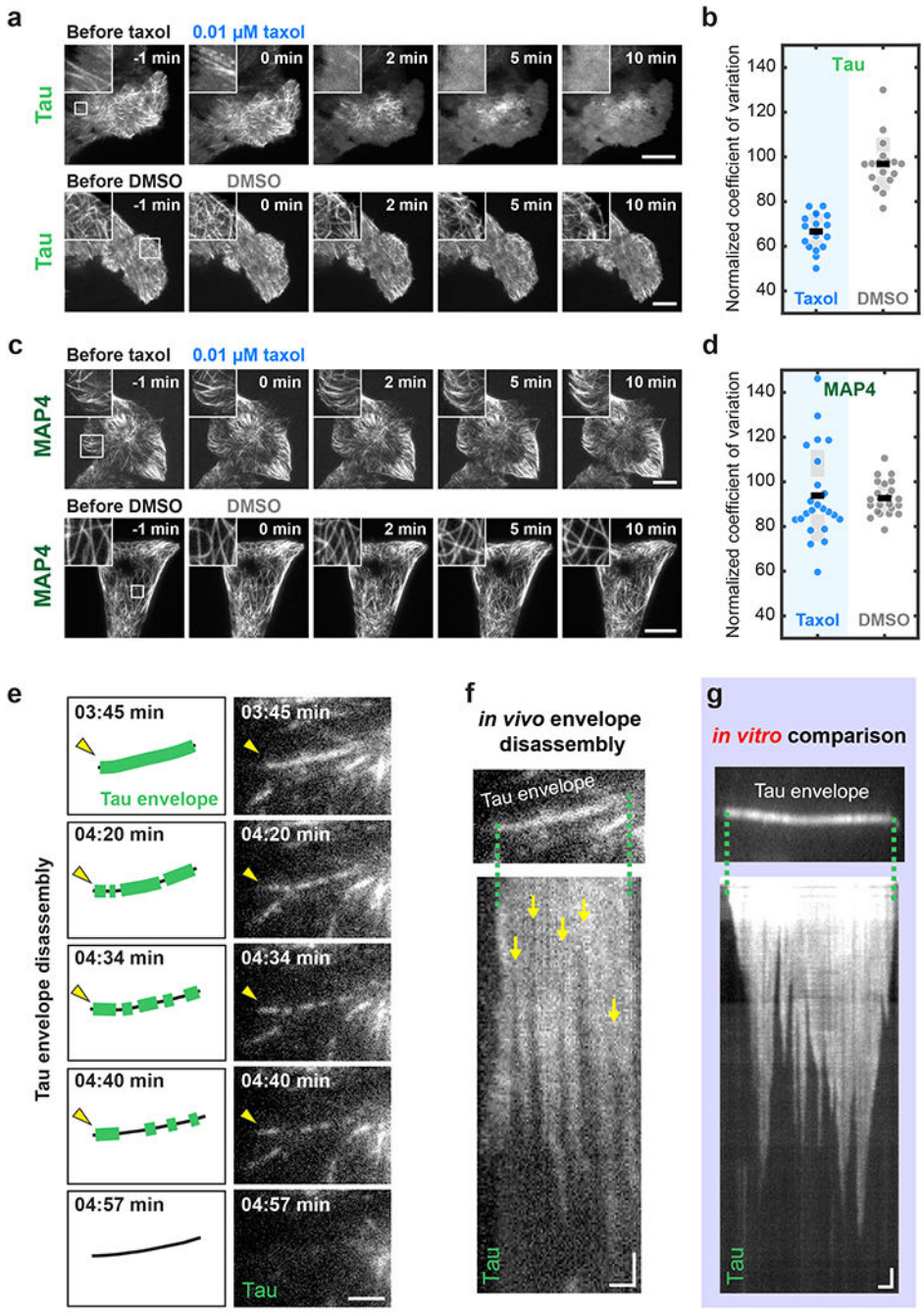

Figure 4: Lattice spacing governs MAP cooperativity in vivo.

a. Time lapse micrographs of U-2 OS cells expressing eGFP-tau treated with 0.01 μM taxol (top panels) or DMSO (bottom panels). Zoom-ins of the indicated region are provided in the top left corner of the original micrograph. Scale bars: 10 μm. **b.** Coefficient of variation of eGFP-tau cells 10 minutes after taxol or DMSO treatment, normalized to the coefficient of variation before treatment (at t=−1 min). Coefficient of variation was calculated over the whole cell (eGFP-tau after taxol treatment: 66.6 ± 8.0 (mean ± s.d.); n = 18 cells, 5 experiments; eGFP-tau after DMSO treatment: 96.8 ± 11.8 (mean ± s.d.); 17 cells,

7 experiments, two-sided t-test, $p<0.0001$). **c.** Time lapse micrographs of U-2 OS cells expressing eGFP-MAP4 treated with 0.01 μM taxol (top panels) or DMSO (control, bottom panels). Zoom-ins of the indicated regions are provided in the top left corner of the original micrograph. Scale bars: 10 μm. **d.** Coefficient of variation of eGFP-MAP4 cells 10 minutes after taxol or DMSO treatment, normalized to the coefficient of variation before the same treatment (at t=−1 min). The coefficient of variation was calculated over the whole cell (eGFP-MAP4 after taxol treatment: 93.8 ± 20.4 (mean ± s.d.); n = 23 cells, 5 experiments; eGFP-MAP4 after DMSO treatment: 92.7 ± 7.5 (mean ± s.d.); n=23 cells, 5 experiments, two-sided t-test, p=0.7936). **e.** Zoom in from movie as shown in **a** showing the progression of tau signal on a single microtubule (yellow arrowhead) initially fully covered by eGFP-tau after taxol treatment. Sketches of the micrographs (panels next to the original micrographs) indicate the size and locations of fissures in tau signal that appear after taxol treatment. Scale bar: 2 μm. **f.** Fluorescence kymograph of the microtubule presented in **e** showing the fissures (yellow arrows) appearing in the eGFP-tau signal and the disassembly of the tau envelopes from their boundaries. Scale bars: horizontal 1 μm, vertical 10s. **g.** Fluorescence kymograph of tau envelope disassembly *in vitro* showing striking resemblance with the *in vivo* observations in **f**. Scale bars: horizontal 2 μm, vertical 10s.

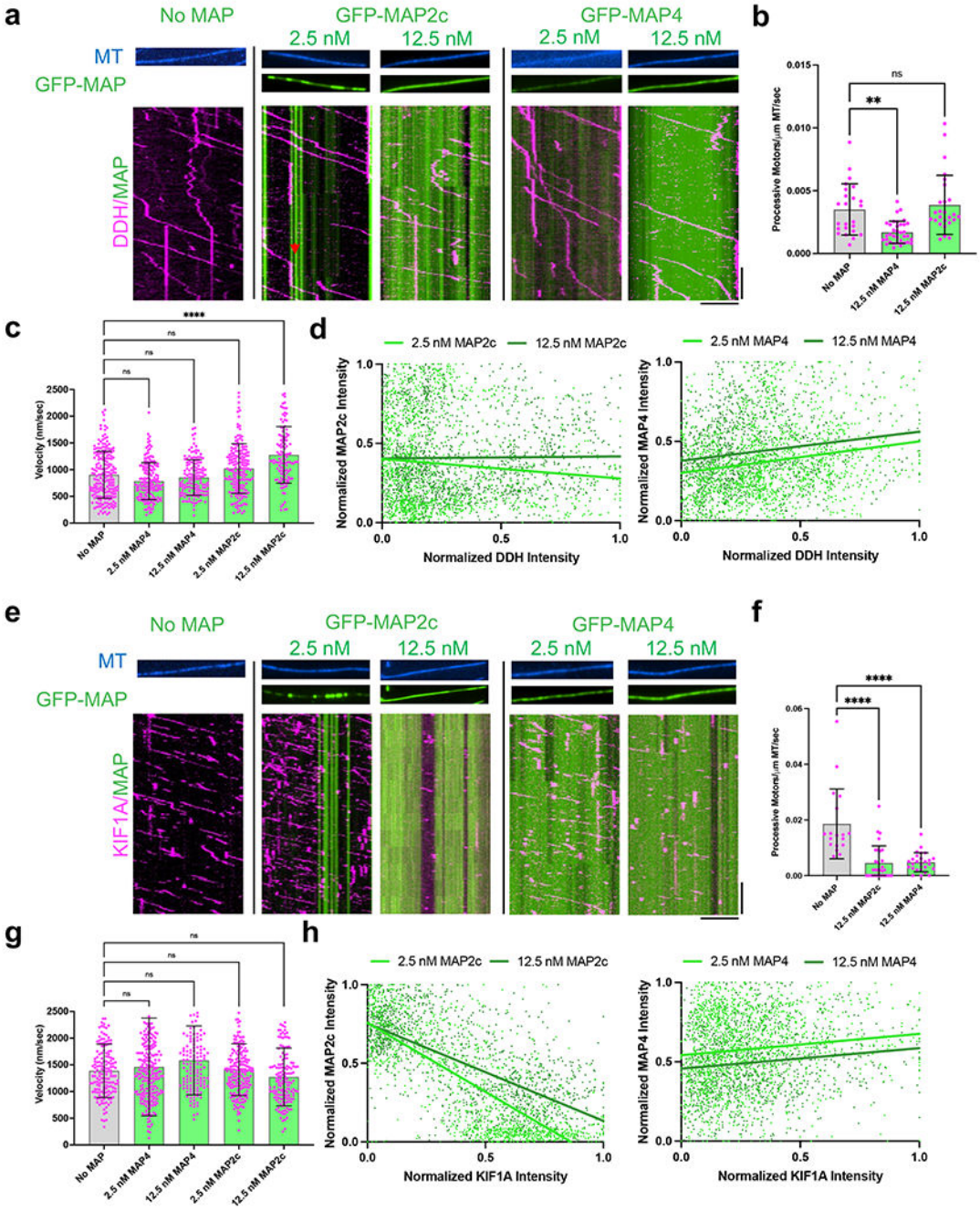

Figure 5: MAP cooperativity results in differential regulation of motor proteins.

a. Fluorescence micrographs showing microtubules (MT) (blue) and GFP-MAPs (green). Below each condition is a representative kymograph showing TMR-DDH (magenta) behavior. Red arrow denotes a pausing event. Scale bars: horizontal 5μm, vertical 10s. Note kymographs do not directly correlate with example images above. **b**. Quantification of the number of processive TMR-DDH complexes observed at the highest concentration of each GFP-MAP examined. Bars show averages with s.d., magenta dots show individual measurement values: n=24, 35, and 26 microtubules quantified from two independent

trials each. ** p=0.0014, ns- not significant by one-way ANOVA. **c.** Quantification of TMR-DDH velocities in the indicated conditions. Bars show averages with s.d., magenta dots show individual measurement values: n=201, 174, 143, 175, and 121 DDH complexes respectively, 2 experiments each. **** p<0.0001, ns- not significant by one-way ANOVA. **d.** Graphs displaying individual xy pairs per pixel for average GFP-MAP2c or GFP-MAP4 intensity versus average TMR-DDH intensity along the microtubule, fit with linear regression. Pearson's correlation coefficients: −0.09669 and 0.01279 for 2.5 and 12.5 nM MAP2c respectively, and 0.1957 and 0.1671 for 2.5 and 12.5 nM MAP4 respectively. n=1337 and 1557 xy pairs from n=10 microtubules, 2 experiments for 2.5 nM and 12.5 nM MAP2c. n = 1648 and 1193 xy pairs from n = 10 microtubules, 2 experiments for 2.5 and 12.5 nM MAP4. p= 0.004, 0.6121, <0.001, and <0.001 for each 2.5, 12,5, 2.5, and 12.5 nM MAP2c and MAP4, respectively. **e.** Representative fluorescence micrographs showing microtubules (MT) (blue) and GFP-MAPs (green). Below each condition is a representative kymograph showing mScarlet-KIF1A (magenta) behavior. Scale bars: horizontal 5μm, vertical 10s. **f.** Quantification of the number of processive mScarlet-KIF1A motors observed at the highest concentration of each GFP-MAP examined. Bars show averages with s.d., magenta dots show individual measurement values: n=18, 26, and 30 microtubules, 2 experiments each. ****p<0.0001 by one-way ANOVA. **g.** Quantification of mScarlet-KIF1A velocities in the indicated conditions. Bars show averages with s.d., magenta dots show individual measurement values: n=158, 235, 138, 199, and 151 KIF1A motors respectively, 2 experiments each. ns- not significant by one-way ANOVA. **h.** Graphs displaying individual xy pairs per pixel for average GFP-MAP2c or GFP-MAP4 intensity versus average mScarlet-KIF1A intensity along the microtubule, fit with linear regression lines. Pearson's correlation coefficients: −0.7620 and −0.6709 for 2.5 and 12.5 nM MAP2c respectively, and 0.1237 and 0.1201 for 2.5 and 12.5 nM MAP4, respectively. n=1243 and 1354 xy pairs, 10 microtubules, 2 experiments for 2.5 nM and 12.5 nM MAP2c. n=1574 and 1121 xy pairs, 10 microtubules, 2 experiments for 2.5 and 12.5 nM MAP4. p= <0.0001, <0.001, <0.0001, and <0.0001 for each 2.5, 12,5, 2.5, and 12.5 nM MAP2c and MAP4, respectively.